A database of radiogenic Sr-Nd isotopes at the "three poles"

Zhiheng Du[a], Jiao Yang[a], Lei Wang[b], Ninglian Wang[c], Anders Svensson[d], Zhen Zhang[e], Xiangyu Ma[f], Yaping Liu[a], Shimeng Wang[a], Jianzhong Xu[a], Cunde Xiao[b*]

[a]State Key Laboratory of Cryospheric Science, Northwest Institute of Eco-Environment and Resources, Chinese Academy of Sciences, Lanzhou 730000, China

[b]State Key Laboratory of Earth Surface Processes and Resource Ecology, Beijing Normal University, Beijing 100875, China

[c]College of Urban and Environmental Sciences, Northwest University, Xi'an 710127, China

[d]Centre for Ice and Climate, Niels Bohr Institute, University of Copenhagen, Copenhagen, Denmark

[e]School of Spatial Informatics and Geomatics Engineering, Anhui University of Science and Technology, Huainan 232001, China

[f]Qingdao Blue Thinking Information Technology Co.Ltd, Qinggao 266555, China

*Correspondence and requests for materials should be addressed to CD. X (cdxiao@bnu.edu.cn).

Abstract: The radiogenic isotope compositions of strontium (Sr) and neodymium (Nd) on the surface of the Earth are powerful tools for tracing dust sources and sinks on Earth's surface. To differentiate between the spatial variabilities of aeolian dust sources in key cryospheric regions at the three poles (including the 'Third Pole' covering the high mountainous area in Asia, the Arctic and Antarctica), a dataset of the Sr-Nd isotopic compositions from the terrestrial extremely cold or arid environments in this study was compiled, similar to the method of Blanchet (2019).

26 The database identified snow, ice, sand, soil (loess), sediment, and rock from the

27 modern and Quaternary periods of the three poles based on 90 different references and

28 our own measurement data, with a total of 1989 data points, 206 data points with

29 different grain sizes and 212 data points with fraction measurements. There are 485

30 data points from the Third Pole, 727 data points from the Arctic, and 777 data points

31 from the Antarctica. The sampling and measurement methods of these data are

32 introduced. For each pole, geographical coordinates and other information are

33 provided. The main scientific purpose of this dataset is to provide collective

34 documentation and our own measurements for the Sr-Nd dataset, which will be useful

35 for determining the sources and transport pathways of dust in snow and ice, river, and

36 oceans at the three poles, and to investigate whether multiple dust sources are present

37 at each of the poles. This dataset provides exhaustive detailed documentation of the

38 isotopic signatures at the three poles during specific time intervals of the Quaternary

39 period, which are useful for understanding the sources or sinks of aeolian dust or

40 sediments at the three poles. The datasets are available from the National Tibetan

41 Plateau Data Center (https://doi.org/10.11888/Cryos.tpdc.272100, Du et al., 2022).

42 **Keywords**: Radiogenic isotopic dataset, Third Pole, Arctic Ocean, Southern Ocean,

43 Greenland and Antarctic ice sheets, Dust provenances.

44 **1. Introduction**

45   The role of mineral dust in the Earth system extends well beyond its impact on

46 the energy balance and involves interactions with the carbon cycle and glacier melting

47 on global scales (Skiles et al., 2018; Shao et al., 2011). The transport of dust from the

48 low mid-latitudes, which contain major deserts that are dust sources, to the Arctic

49 region or AIS is sensitive to amplified high-latitude climatic variability (Bory et al.,

50 2003a; Bory et al., 2003b; Lupker et al., 2010; Lambert et al., 2013: Struve et al.,

51 2020). The isotopic compositions of the radiogenic isotopes strontium (Sr) and

52 neodymium (Nd) are powerful tools for tracing dust sources and sinks because their

53 characteristics are significantly different on the surface of the Earth (including snow,

54 sand, sediment, loess and aeolian deposits) (Grousset et al., 2005; Chen et al., 2007;

55 Xu et al., 2012; Robinson et al., 2021). Therefore, the combination of different

56 isotopic signatures, specifically $^{87}Sr/^{86}Sr$ and $^{143}Nd/^{144}Nd$ (expressed as $\varepsilon_{Nd}(0)$), has

57 proven to be useful in discriminating different dust source areas in Earth science.

58   The transport of aeolian dust from natural desert regions has also been identified

59 in modern snow and ice records at the third pole based on Sr-Nd data (Wu et al., 2010;

60 Xu et al., 2012; Du et al., 2015; Dong et al., 2018). Many studies have focused on

61 dust transport from the western Chinese deserts to the Chinese loess plateau (CLP),

62 Pacific Ocean and even the Greenland ice sheet (GrIS) (Biscaye et al., 1997; Chen et

63 al., 2007; Wei et al., 2021). However, it is still a controversial issue; for example,

64 recent results have emphasized that aeolian dust from local sources contributes

65 significantly to high mountain glaciers (Du et al., 2019a; Wei et al., 2021). And

66 aeolian dust from various source regions, including the Saharan Desert in North

67 Africa and the Gobi and Taklimakan Deserts in Asia, is transported to the Greenland

68 snow and ice, and there are still great uncertainties (Han et al., 2018).

69   The Sr-Nd data in snow layers at the Berkner Island ice sheet in western

70 Antarctica, for most of the year, are data support scenarios that involve contributions

71 from proximal sources (Bory et al., 2010). The Sr-Nd data from insoluble dust in

72 snow samples from East Antarctica indicate that long-distance natural dust primarily

73 originates from Australia and that local dust originates from ice-free areas (Du et al.,

74 2018). The Sr-Nd data in the Taylor Glacier zero-age ice samples and snow samples

75 from Roosevelt Island could be a mixture of at least two local sources (Winton et al.,

76 2016; Aarons et al., 2017). The Sr-Nd data from East Antarctica ice cores during the

77 Holocene indicate a well-mixed atmospheric background involving a mixture of two

78 or more sources in the Southern Hemisphere (SH) (Aarons et al., 2016, 2017;

79 Delmonte et al., 2019). The amount of isotopic information is currently adequate for

80 Patagonian and non-Patagonian mineral dust exported from southern South America

81 and the East Antarctic ice sheet (EAIS) (Grousset et al., 1992; Gaiero et al., 2007;

82 Delmonte et al., 2010a, b, 2019; Delmonte et al., 2013; Blakowski et al., 2016; Aarons

83 et al., 2017). Major efforts have attempted to solve the 'puzzle' of the origin of the

84 potential source areas that contribute dust to the Southern Ocean (SO) and the whole

85 Antarctic Ice Sheet (AIS) (Gili et al., 2021). However, Sr-Nd data in the entire AIS

86 have an uneven distribution. Measuring Sr-Nd stable isotopic compositions in ice

87 cores from Antarctica is a major challenge.

88   As much Sr-Nd data were measured, these data characteristics and measurement

89 methods, which is necessary to reassess these data on the dust sources in these remote

90 regions. Therefore, the amounts of Sr-Nd data measured in snow, soil, sediment, sand

91 and other samples should be integrated into a dataset to better serve the environmental

92 and climatic sciences studying the third regions in the future. The answers to these

93 questions have been hindered by a paucity of Sr-Nd data, which provide information

94 on the local and potential dust sources. For these reasons, we measured Sr-Nd data in

95 some samples and collected Sr-Nd data in the literature at the three poles (Fig. 1,

96 Table 1). Therefore, the objective of this work was to produce a compilation of

97 published and unpublished data from the three poles, and the specific time intervals of

98 Sr-Nd data were limited to the Quaternary period. As an example, the modern dust

99 (Holocene) in snow or ice and sediment sample contributions from the three poles

100 were further discussed, and the potential dust transport paths in Greenland and

Antarctic ice sheets were traced. Similar to the method of Blanchet (2019), here, we compile published and unpublished Sr-Nd data with an integrated filtering system from three remote poles, in which these data were collected in extremely cold or arid environments, and most of the data were not included in the previous dataset. The dataset will help trace modern natural dust, reconstruct past environments, and extend the database of terrestrial and marine radiogenic Sr and Nd isotope data in the Earth and environmental sciences.

2. Sample measurement and data processing

2.1 Sample collection and measurement

Sr-Nd data in snow, sand, soil, cryoconite, loess and sediment samples were collected from our own research and literature from the three poles (which refers to the high mountainous regions in Asia, the Arctic and Antarctica) (Fig. 1). Sr-Nd data in the Third Pole cover the area of 40° to 23°N and 106° to 61°E and included data from arid deserts and mountains in northern China (Fig. 2). Sr-Nd data in the Arctic from the high Arctic to the sub-Arctic areas, and Sr-Nd data in Antarctica refer to the area including the entire Antarctic continent, the AIS, and the Antarctic Peninsula (>60°S). Sr-Nd data were collected from Australia, southern South America (SSA), southern Africa (SA) and New Zealand (Fig. 1). The cryoconite samples indicate that the mixtures and/or aggregates of these biotic and abiotic impurities on glacial ice, were collected at different elevations in glaciers (Table 2). Note that the Sr-Nd data from the snow, ice core, surface aeolian dust, deposit samples, and the ages of these samples are almost all less than 1 million years. Therefore, the ages of Sr-Nd data are limited to the Quaternary period in this dataset.

125
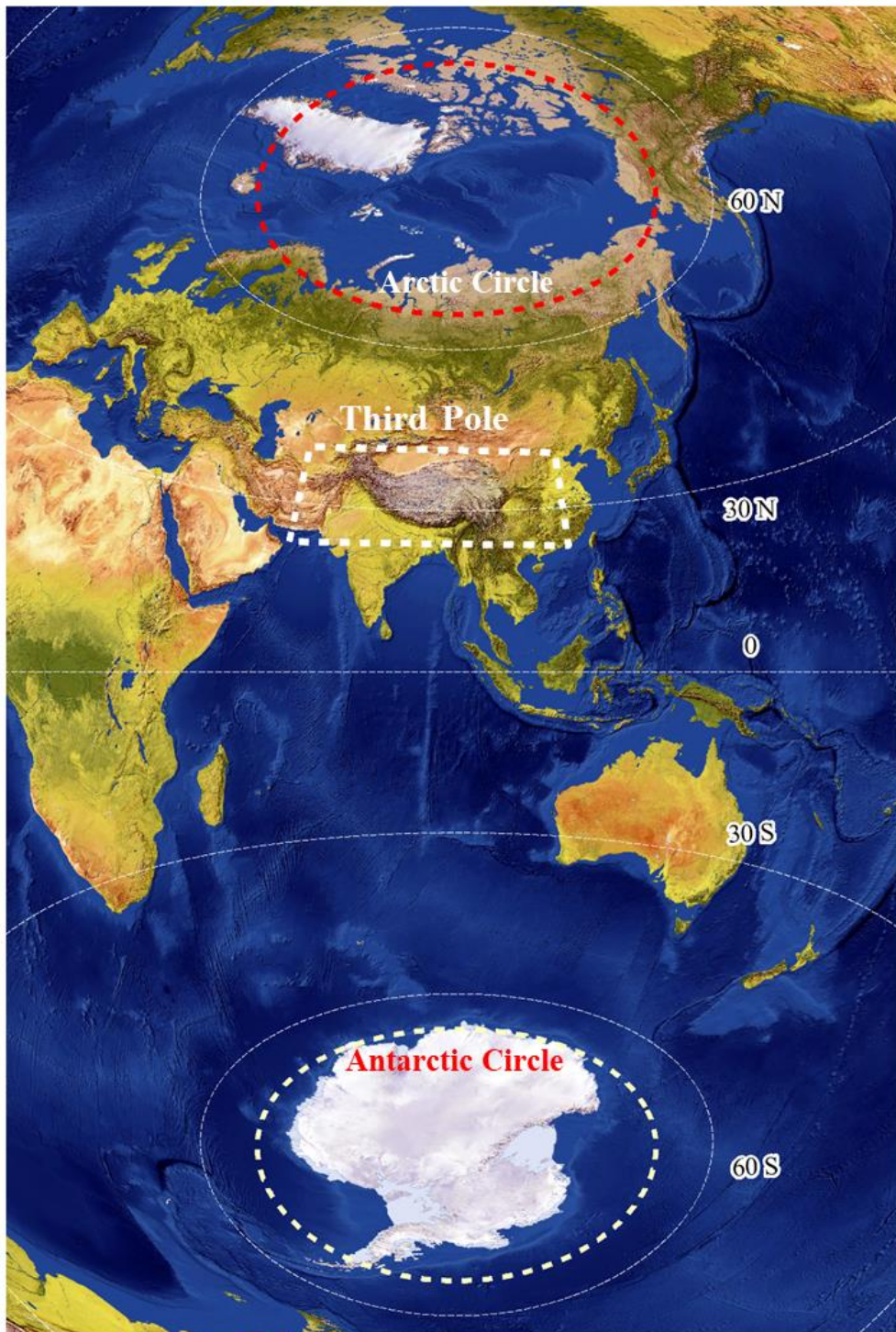
Fig. 1. Map of the sampling regions in the three poles (Third Pole: covering the high mountainous area in Asia, data were collected in the area of 40° to 23°N and 106° to 61°E, Li et al., 2020; Arctic: from the high Arctic to the sub-Arctic areas, data were collected >60°N in this region); and Antarctica: data were collected >60°S in this

130 region, which are indicated with different coloured circles) in this study (The

131 background of this figure is from ArcGIS).

132   Two sand samples from Kangerlussuaq, West Greenland were collected. Four

133 sand samples collected on King George Island and eleven sand samples collected on

134 Inexpressible Island in the Ross Sea, West Antarctica, were measured in this study. In

135 general, the upper 2 or 5 cm of surface topsoil (sand) was collected with a trowel and

136 stored in precleaned plastic bags or bottles. The sediment samples from shelves and

137 ridges in the Arctic Ocean (AO), which were mostly retrieved from core archives,

138 were subsampled in the upper surface of the core tops (with rare exceptions) (Maccali

139 et al., 2018). Different grain sizes (<5 µm, <10 µm, 30 µm, <63 µm, <75 µm and <100

140 µm fractions and bulk) of surface soil or sand were extracted by the sieving method

141 (Chen et al., 2007; Maccali et al., 2018; Du et al., 2018, 2019a, b; Wei et al., 2021).

142   Snow samples were collected from the snowpit at a vertical resolution of 5–20

143 cm, following the clean-hands protocol with sampling personnel wearing integral

144 Tyvek® bodysuits, nonpowdered gloves and masks to avoid possible contamination

145 (Xu et al., 2012). In this study, one 1.0 m snowpit with a resolution of 10 cm was dug

146 in the East Greenland ice sheet (GrIS), and four fresh snow samples (M1, M2, M3 and

147 M4) were sampled on sea ice in the Arctic Ocean (AO) during fulfil mission of the

148 Multidisciplinary drifting Observatory for the Study of Arctic Climate (MOSAIC) in

149 October 2020. Surface fresh snow (2-10 cm) samples at different resolutions (with

150 different thicknesses, widths and lengths) in Greenland and Antarctica ice sheets were

151 excavated and placed in 5 L Whirl-Pak bags (Du et al., 2018; Du et al., 2019a, b).

152 Three horizontal snow layers were collected for Greenland and Antarctica snowpits

153 (Bory et al., 2003b; Bory et al., 2010). The dust in the ice core was extracted using the

154 same method as that for the snow samples. Snow or ice core samples are nearly bulk

155 samples or have different grain sizes (>0.2 μm, > 0.45 μm, > 0.45 μm and <30 μm)

156 (Du et al., 2015, 2019b; Bory et al., 2003 a, b; Bory et al., 2010; Lupker et al., 2010;

157 Wu et al., 2010).

2.2 Data processing

159   Sr-Nd isotope datasets from snow, ice cores, sand, sediment, soil and loess

160 samples from the Third Pole, Arctic and Antarctica were compiled. Data were

161 collected from 90 different references with 2847 data points. In total, 485 data points

162 were collected from the Third Pole, 727 data points were collected from the Arctic,

163 and 777 data points were collected from the Antarctica. In addition, 259 data points

164 were collected from the Pan-third pole (included Tibetan Plateau, Pamir, Hindu Kush,

165 Tienshan, Iranian Plateau, Caucasus, Carpathians, as well as the surrounding deserts),

166 and 181 data points were included from the potential source areas (PSAs) of SH.

167 Details of geographical coordinates and original information can be found in this

168 dataset, and the locations of these samples are shown on maps. To keep the naming

169 scheme uniform, the dataset assembled the names of each sample based on the work

170 by Blanchet (2019). This dataset was built by incorporating data from the literature

171 and our own database; in particular, units, source or sink and geographical coordinates

172 are marked in the dataset. Note that whether the Sr-Nd data represents source or sink

173 information, which need be further determined by the detail depositional environment

174 or distributed locations. For examples, the loess samples from the CLP represent the

175 sink, which they also represent the dust source for the Pacific Ocean. Therefore, these

176 samples were marked with mixture. And the sediment samples from the coast of SO

177 or AO (Rivers or Dune sand) were also marked with mixture. An overview of the

178 input data is shown in Table 1. The study focuses on the large amounts of different

179 data, including data on snow, ice, sand, soil, loess, sediment, etc. The data are based

180   on our own measurements, author contributions (data published) and literature

181   searches.

182   All subsequent procedures were performed in clean lab facilities. The sand, loess,

183   sediment, cryoconite and dust extracted from snow or ice cores were generally

184   digested with ultrapure acid (HNO_3, HF and $HClO_4$ or HNO_3, HF and HCl), and

185    $^{87}Sr/^{86}Sr$ and $^{143}Nd/^{144}Nd$ ratios were determined by the different types of

186   thermoionization mass spectrometry or multiple collector inductively coupled

187   plasma-mass spectrometry. Sr-Nd values, with uncertainties expressed as $\pm 2\sigma \times 10^{-6}$ (2

188   standard errors of the mean), can also be found in the original references. The

189    $^{143}Nd/^{144}Nd$ isotopic composition is expressed as:

190    $\varepsilon_{Nd}(0) = ((^{143}Nd/^{144}Nd)_{Sample}/(^{143}Nd/^{144}Nd)_{CHUR}-1) \times 10^4$, where $(^{143}Nd/^{144}Nd)_{CHUR}$

191    $= 0.512638$, where CHUR stands for chondritic uniform reservoir and represents a

192   present-day average Earth value $(^{143}Nd/^{144}Nd)_{CHUR}=0.512638$ (Jacobsen &

193   Wasserburg 1980).

194   **3. Data descriptions**

195   **3.1. Reliability assessment for the differences in Sr-Nd based on grain sizes,**

196   **lithogenic and measuring methods**

197   The grain size effect in different samples resulted in $^{87}Sr/^{86}Sr$ ratio and $\varepsilon_{Nd}(0)$

198   variations. For surface aeolian sand and marine sediment samples, the variations in

199   size-separated $^{87}Sr/^{86}Sr$ values are affected by grain size (Chen et al., 2007; Tütken et

200   al., 2002). The Sr isotope ratios in loess from the CLP tended to be higher in the fine

201   fraction and were much higher in the <2 µm fraction than in other coarser fractions

202   (Rao et al., 2006). However, the variations in the $^{87}Sr/^{86}Sr$ isotopic ratios in alpine

203   soils of the Tibetan Plateau are not clearly related to the grain size effect (Lin and

204   Feng, 2015). $\varepsilon_{Nd}(0)$ values clearly exhibits less grain size-dependent variability,

because $\varepsilon_{Nd}(0)$ values seem not to be fractionated between mineralogically different grain-size fractions during the sedimentary cycle (Tütken et al., 2002). While a substantial proportion of Sr-Nd isotope values showed enrichment in the coarse-grained fraction, which is accounted for by source-rock types (Xie et al., 2020). Within the isotopically diverse Indus delta sediment, bulk isotopic compositions are estimated to deviate on average no more than ±1.04 ε_{Nd} units and ±0.0099 for $^{87}Sr/^{86}Sr$ values for any sediment as a result of mineralogy, grain size distribution, and analytical error (Jonell et al., 2018).

The $\varepsilon_{Nd}(0)$ signatures of the lithic fraction of the sediments are taken as a robust circulation and hydrologic proxies applicable because of its different origins across timescales (Revel et al., 1996; Abbott et al., 2022). However, Sr-Nd isotope ratios in the lithogenic sediment fraction represent a complex mixture (Meinhardt et al., 2016; Bayon et al., 2021). The widespread influence of lithogenically sourced neodymium on authigenic $\varepsilon_{Nd}(0)$ had been demonstrated. Such as, there is a strong linear relationship between detrital $\varepsilon_{Nd}(0)$ and authigenic $\varepsilon_{Nd}(0)$ (r=0.86, n=871) (Abbott et al., 2022). Therefore, the sediment characteristics and detrital isotope records should be considered when used $\varepsilon_{Nd}(0)$ data. The different acid leaching methods also have an effect on the Sr-Nd isotopic composition in the silt and clay fractions in marine sediments (Walter et al., 2000). Loess samples from the CLP and cryoconites (including surface dust) from high mountain glaciers had obviously higher $^{87}Sr/^{86}Sr$ ratios in acid treatment materials than without acid treatment or bulk sample (Rao et al., 2006; Nagatsuka et al., 2010, Nagatsuka et al., 2019).

Therefore, assuming that Sr-Nd data in different media in this dataset were used for interpreting Sr-Nd isotope compositions in terms of provenance, the grain sizes, lithogenic and measurement methods on these isotopic data must be considered for

230   better illustration using these data.

3.2 The Sr-Nd data characteristics of glaciers at the Third Pole

232   Table 2 and Fig. 2 provide an overview of the information (the serial number of

233   glaciers; sub-regions; glacier name; name of the sampling site where the samples were

234   taken; sample type, age, elevation; longitude and latitude and elevation) from the

235   Third Pole. The dust in snow or ice in the Third Pole absolutely originates from PSAs,

236   therefore, Sr-Nd data in these samples represents the characteristics of sinks. And

237   Sr-Nd data from the local or arid deserts sand or soil represents the characteristics of

238   PSAs. As an example, the isotopic signatures in insoluble dust of these snow/ice

239   (sinks) from the Third Pole can be traced that which originate from the possible PSAs

240   based on those Sr-Nd data and geographic characteristics in sand (soil) samples from

241   the local exposed bedrock and long-distance dust transport of arid deserts. The same

242   Sr-Nd measurement methods were used in these snow samples (Xu et al., 2012; Du et

243   al., 2015, 2019a; Dong et al., 2018, Wei et al., 2019, 2021), and a similar

244   measurement method was used in those sand or surface dust samples (Chen et al.,

245   2007; Nagatsuka et al., 2010). The data results seem to remain fully consistent with

246   these references.

247   The sorting criteria for determining PSAs based on mountains and glaciers

248   distribution, geographic features and isotopic values (snow or ice from the Third Pole

249   glaciers, sand (soil) from local and arid deserts), six isotopic sub-regions across the

250   entire Third Pole were divided as follows (Fig. 2):

251   Region I: Samples from glaciers located in the Altai Mountains include snow

252   samples from Musidao glacier and Altay, and sand samples from the Gurbantunggut

253   Desert, with $\varepsilon_{Nd}(0)$ values from -6.6 to -1.2 and $^{87}Sr/^{86}Sr$ values ranging from

254   0.705483 to 0.71480. The highest $\varepsilon_{Nd}(0)$ values were observed in this region (Chen et

255 al., 2007; Xu et al., 2012; Du et al., 2019a).

256 Region II: Samples from the glaciers on the northern margin of the TP include

257 snow samples from the Tienshan Mountains (Tienshan No. 1 glacier and Miaoergou

258 ice cap) and Kunlun Mountains (Muztagata), as well as sand samples from the

259 Taklimakan Desert, with $\varepsilon_{Nd}(0)$ values from -11.8 to -6.9 and $^{87}Sr/^{86}Sr$ values from

260 0.70842 to 0.728641 (Chen et al., 2007; Nagatsuka et al., 2010; Du et al., 2015; Xu et

261 al., 2012; Wei et al., 2019).

262 Region III: The Sr-Nd isotopic characteristics of the glaciers and sand/soil in the

263 interior of the TP include $\varepsilon_{Nd}(0)$ values ranging from -10.5 to -8.6 and $^{87}Sr/^{86}Sr$ values

264 from 0.713192 to 0.721786 (Xu et al., 2012; Du et al., 2019a; Wei et al., 2021).

265 Region IV: The Sr-Nd isotope data from snow and sand (soil) samples from

266 glaciers in the Himalayan Mountains (East Rongbuk, Jiemayangzong and Yala)

267 include $\varepsilon_{Nd}(0)$ values ranging from -28.1 to -10.5 and $^{87}Sr/^{86}Sr$ values ranging from

268 0.724542 to 0.757407 (Xu et al., 2012; Wei et al., 2021).

269 Region V: Samples from the glaciers in the Qilian Mountains include snow

270 samples from the Qilian Mountains and sand (soil and loess) samples from the Hexi

271 Corridor, with $\varepsilon_{Nd}(0)$ values from -15.7 to -7.0 and $^{87}Sr/^{86}Sr$ values from 0.712349 to

272 0.73211 (Wei et al., 2017; Dong et al., 2018). The $\varepsilon_{Nd}(0)$ values have an increasing

273 trend along the Hexi Corridor from west to east: -15.7–-12.9 for Laohugou No. 12

274 glacier (local soil: -13.6), -13.7–-8.58 for Qiyi, -13.8–-13.6 for Shiyi glacier (local

275 soil: -13.8–-13.6), -12.1–-12.0 for Dabanshan snowpack, and -10.9–-7.0 for

276 Lenglongling glacier (Fig. 2, Dong et al., 2018). It is very clear that, based on local

277 soil data, regional dust makes a significant contribution to these glaciers.

278 Region VI: Samples from the glaciers in the eastern TP include snow and soil

279 samples from the Hengduan Mountains, with $\varepsilon_{Nd}(0)$ values from -17.1 to -10.1 and

^{87}Sr/^{86}Sr values from 0.717145 to 0.735863 (Xu et al., 2012; Dong et al., 2018).

There is an increasing ^{87}Sr/^{86}Sr trend from north (region I) to south (region V), and there is a decreasing $\varepsilon_{Nd}(0)$ trend from north (region I) to south (region V). The maximum ^{87}Sr/^{86}Sr ratios and minimum $\varepsilon_{Nd}(0)$ values were observed in region V (Fig. 3). The Sr-Nd data in the Third Pole have relatively narrow ranges with distinct features, while the largest uncertainty was observed from Region IV (Fig. 3).
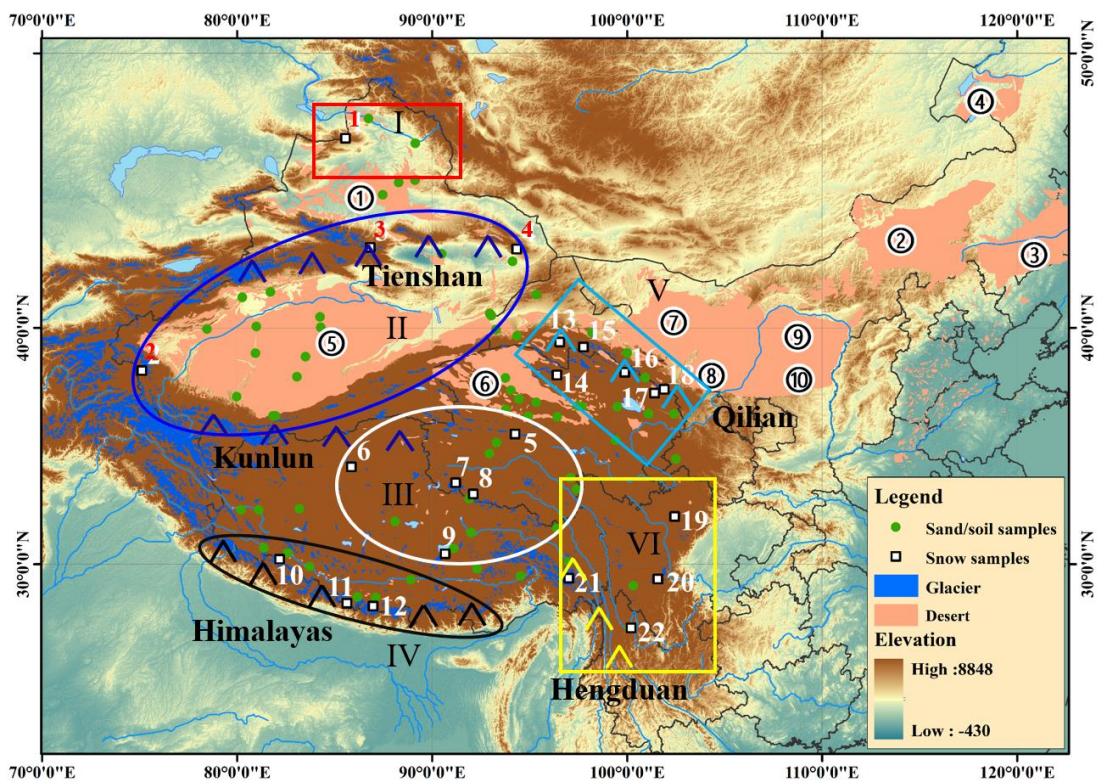
Fig. 2. The glacier and desert distributions in western China (the different coloured oval and rectangular shapes represent six sub-regions (PSAs and glaciers) (Tienshan, Kunlun, Qilian, Himalayas and Hengduan Mountains) in the Third Pole; numbers and white rectangles represent 22 glaciers (snow samples were collected from these glaciers) for which the names of glaciers are shown in Table 2, and the numbered circles represent the ten deserts or sandy areas of China (1. Gurbantunggut Desert, 2. Onqin Daga sandy land, 3. Horqin sandy land, 4. Hunlun Buir sandy land, 5. Taklimakan Desert, 6. Qaidam Desert, 7. Badain Jaran Desert, 8. Tengger Desert, 9.

295 Hobq Desert, 10. Mu Us Desert), and green solid circles represent sand/soil samples

296 (this figure was created with ArcGIS).
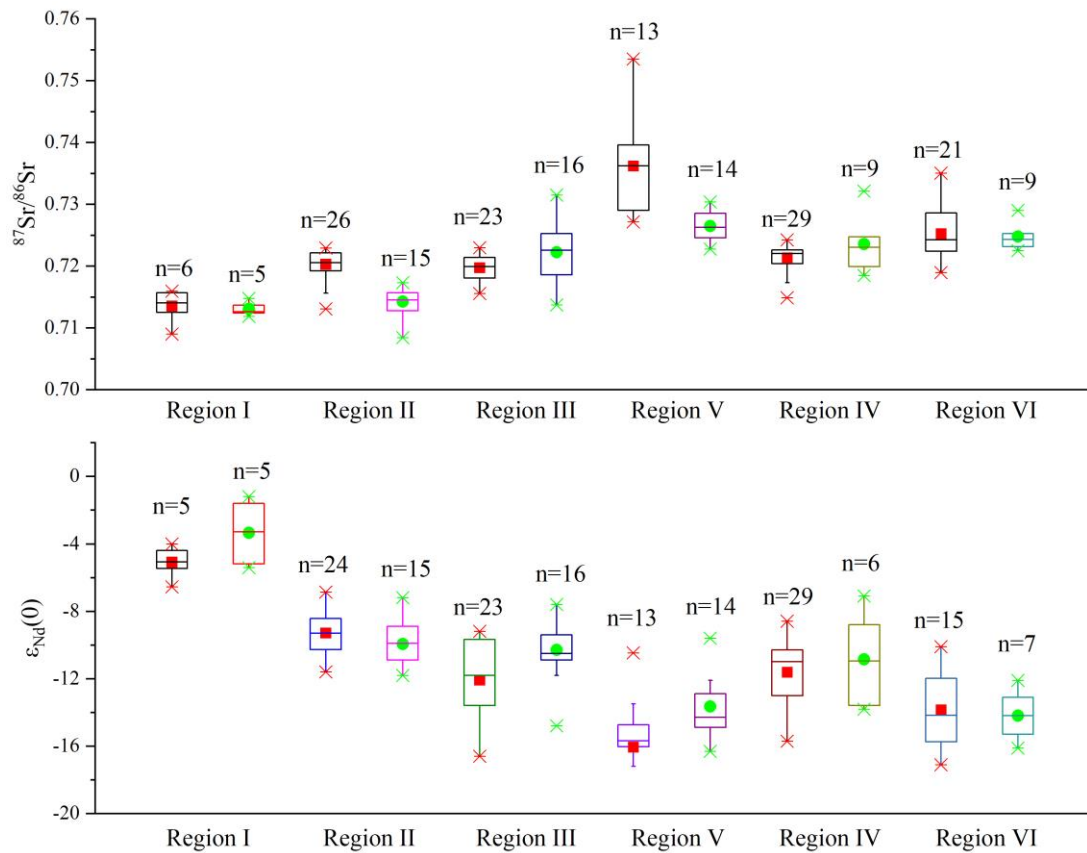
297

298 Fig. 3. Box plot for the Sr-Nd isotope signatures of third pole PSAs and snow samples.

299 Samples are located in each PSA region based on the data from Table 2 (the number

300 of samples for each sub-region are presented (n>5)). The horizontal line within the

301 box is the median, and the squares are the mean Sr-Nd values (red rectangles for sand

302 or soil samples and green solid cycles for snow samples). The interquartile range is

303 represented by the lower and upper boundaries of the boxes, and whiskers indicate

304 confidence intervals of 1.5 times the interquartile range.

305 **3.2. Sr-Nd data from the Arctic**

306 Considerable Sr-Nd data have been obtained from modern snow/ice samples

307 from the Arctic and surface (including sea ice-transported sediments) sediment from

the AO, which covers the entire Arctic and represents the characteristics of sinks (Fig. 4). The data points are presented in Table 3. Sr-Nd data from arid deserts (East Asian and Saharan deserts) have been compiled in previous datasets (Blanchet et al., 2019; Robinson et al., 2021), and these data are useful for tracing terrigenous material transport in the Arctic. For user-friendly selection of the Sr-Nd data according to the modern environment characteristics and the geographical location, Sr-Nd data from the deep ice core are not included in Fig. 5. We compared the Sr-Nd data from the surface snow (sink) and marine sediment (sink or source) samples in the Arctic (Figs. 5 and 6). Based on the isotopic signals of these samples, geologic units, adjacent seas and drainage basins of the main river systems in the Arctic, the Sr-Nd patterns can be divided into 12 sub-regions according to Maccali et al. (2018).
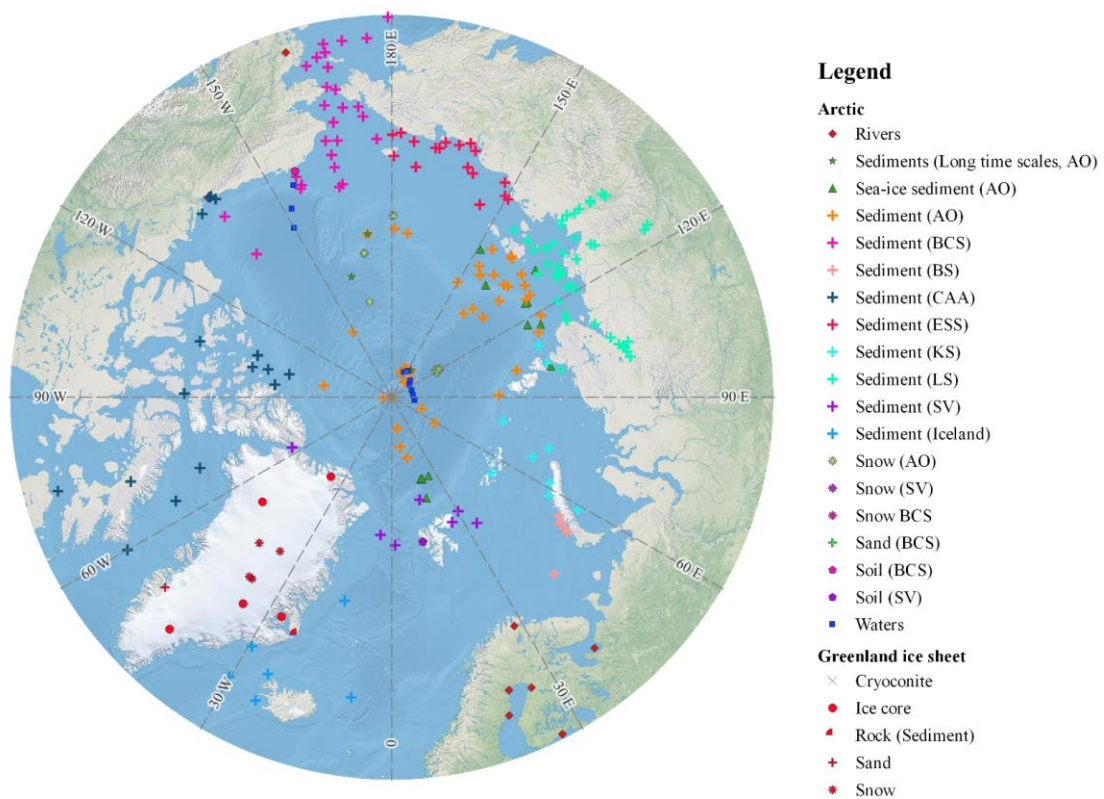
Fig. 4. Sampling distribution sites in the Arctic. The types of samples are denoted with different shapes and colours (Table 3). (AO: Arctic Ocean; BCS: Bering-Chukchi Sea; BS: Barents Sea; CAA: Canadian Arctic Archipelago; ESS: East Siberian Sea;

323   KS: Kara Sea; LS: Laptev Sea; SV: Svalbard) (this figure was created with ArcGIS).

324   **3.2.1 Sr-Nd data from snow/ice and sand samples of the Greenland ice sheet**

325   Sr-Nd data from the East Greenland Ice Core Project (EGRIP) and the North

326   GRIP (NGRIP) were measured via snowpits. Sr-Nd data were also measured in GRIP,

327   GISP2 and NEEM ice cores, and Renland, Site A, Hans Tausen and Dye 3 shallow ice

328   cores. Sr-Nd data exhibit large differences in these samples (Fig. 5). The Sr-Nd data

329   indicated that the dust sources were variable and showed complicated dust sources in

330   the same location for NGRIP snow (Bory et al., 2002; Bory et al., 2003b). As much

331   more Sr-Nd data from the sand, soil, cryoconite, moraine, and englacial dust samples

332   in the periphery of the GrIS were recently measured (Nagatsuka et al., 2016), $^{87}Sr/^{86}Sr$

333   values are high and the $\varepsilon_{Nd}(0)$ values are the least radiogenic in these samples (Table

334   3). Compared with Sr data in NGRIP and EGRIP snowpits (Bory et al., 2002; Bory et

335   al., 2003b), much larger variations were observed for $^{87}Sr/^{86}Sr$ in the EGRIP snowpit,

336   and relatively lower $^{87}Sr/^{86}Sr$ values were observed in the NGRIP snowpit. The $\varepsilon_{Nd}(0)$

337   values in the interior of the GrIS are relatively consistent, while the large differences

338   are observed at the periphery of the GrIS. Therefore, although the Sr-Nd isotope ratios

339   indicated that Asian deserts might be the main dust source for the GrIS, the ice-free

340   region around the GrIS might be another source for the interior GrIS. Sr-Nd data in

341   sediment samples collected from the Scoresby Sund region by Simonsen et al. (2019)

342   are as follows: the $^{87}Sr/^{86}Sr$ ratios range from 0.709689 to 0.736137, and the $\varepsilon_{Nd}(0)$

343   values range from -15.7 to -10.1. Combining Sr-Nd values in snow (Renland, Site A,

344   Hans Tausen and Dye 3) and Dye 3 shallow ice core samples, as proposed by Lupker

345   et al. (2010), the local dust sources may contribute some of the dust to the inland

346   regions and the Sahara is also the most likely additional PSA. Thes local dust for the

347   free ice of the GrIS may have been neglected in previous studies.
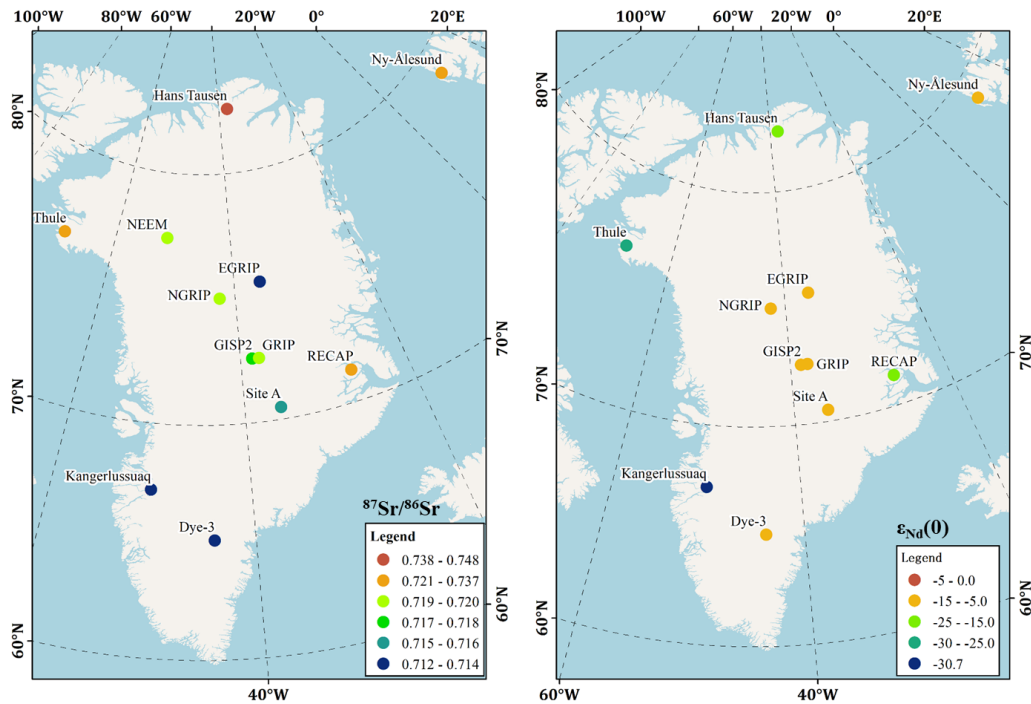
Fig. 5. $^{87}Sr/^{86}Sr$ and $\varepsilon_{Nd}(0)$ data in snow or ice cores, and sand/soil samples from Ny-Ålesund, Svalbard and GrIS (this figure was created with ArcGIS).

The mainstream view of the provenance of dust in inland Greenland deep ice cores (GISP2 and GRIP) is that the dust is from the eastern Asian deserts (the Gobi and Taklimakan Deserts) based on the best Sr-Nd data matches during the last glacial period (Biscaye et al., 1997; Svensson et al., 2000; Újvári et al., 2015). High-resolution Sr isotope data from the Greenland NEEM ice core suggested that there was a significant Saharan dust influence in Greenland during the last glacial period (Han et al., 2018). The Sr-Nd data (>5 μm) in Holocene RECAP ice core samples are attributed to proximal dust sources; however, the resolution of the data is approximately one thousand years (Simonsen et al., 2019). However, the Sr-Nd data in Greenland deep ice core samples (Biscaye et al., 1997; Svensson et al., 2000), which have low resolutions and represent multiyear averages with no seasonal or interannual variations (60 to 200 cm or 30-150 years), need to be considered when

363   using some data.

3.2.2 Sr-Nd data from snow and sediment samples in the Arctic Ocean

365   Surface aeolian dust from mid- or high-latitude continental weathering and arid

366   deserts may be the most important dust contributor to snow and ice cores. The

367   $^{87}Sr/^{86}Sr$ values are higher and $\varepsilon_{Nd}(0)$ values are lower in snow and sand samples from

368   Ny-Ålesund, Svalbard (SV) (not including data from Iceland in Fig. 6). The Sr-Nd

369   data in snow samples from sea ice were measured in bulk, and four of these samples

370   were collected near the North Pole in the western AO by MOSAIC (October 2020) in

371   this study (Figs. 4 and 6). The $\varepsilon_{Nd}(0)$ data have much more negative $\varepsilon_{Nd}(0)$ values

372   (-20.8 to -19.6), which cannot be explained by low latitude potential dust sources. As

373   shown in Fig. 6, the lowest ε_{Nd} values were observed along the ice-free periphery of

374   the GrIS and SV; therefore, these ice-free regions are potential dust sources for natural

375   dust in the AO.

376
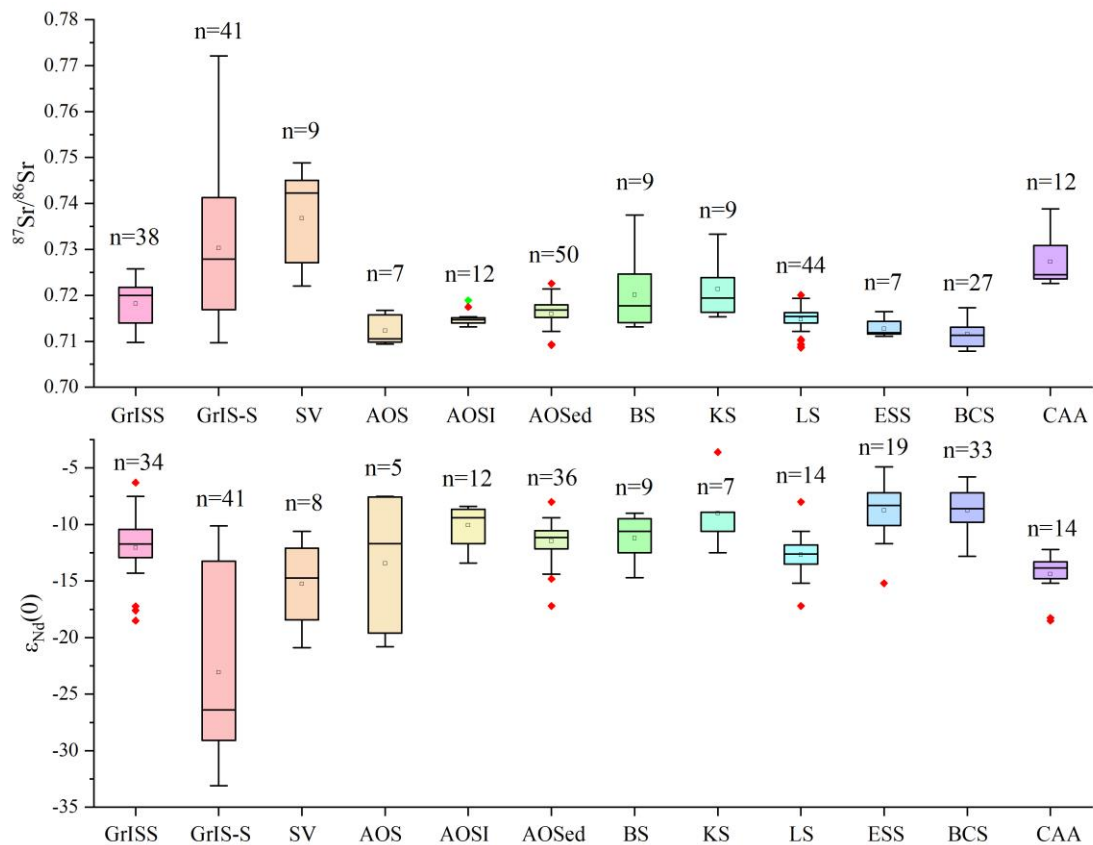
Fig. 6. Box plot for the Sr-Nd isotopic signatures of the Arctic, including the 12 sub-region samples of snow, sand, soil, sediment from sea ice and sediment cores in dataset (the number of samples for each sub-region are presented (n>5)). (GrIS: Greenland ice sheet (snow samples); GrIS-S: Greenland ice sheet (sand); SV: Svalbard (snow and sand); AOS: Arctic Ocean (sediment); AOSI: Arctic Ocean (sea ice sediment)).

The terrigenous material from the Arctic margin sea, including BS, KS, LS, ESS, BCS and CAA, was transported and deposited into the AO, which may be the primary material source for marine sediment. The Sr-Nd data from Arctic surface sediments were based on the literature (Fig. 6), and most samples were sieved at < 45 or 63 μm for bulk sediment samples. These samples were chosen at the surface or 0-10 cm from the top to better represent the characteristics of coastal terrestrial sources as presented by Maccali et al. (2018). The Sr-Nd values from the sediment samples (including sea ice sediment) are almost the same as those of snow samples from the AO, indicating that the same PSAs exist in the central AO. The Sr-Nd signals in sediment from the AO seem to be close to the BS, KS and LS values, which may contribute to the Transpolar Drift originating from the Siberian shelves and crossing the AO towards the Fram Strait. The sample spatial coverage in each sub-region is variable, and Fig. 6 shows the distinguishing characteristics for each region, but Sr-Nd isotopic values overlap for close geographical regions to the greatest extent. Therefore, these data should be carefully used in the different regions.

3.3. Information on Sr-Nd data from the SH and Antarctic ice sheet

By integrating the literature and adding data with new evidence, dust provenances of low-elevation areas on the periphery of the AIS in the Holocene (including modern) were discussed. The dataset provides a comprehensive overview

402   of the state of knowledge of dust sources and sinks in different sectors of the AIS and

403   PSAs in the SH. The location Sr-Nd datasets from different sectors of Antarctica and

404   AIS are presented in Fig. 7. Sr-Nd data from Antarctica are not evenly distributed, and

405   more data were measured in western Antarctica and the Ross Sea. Sr-Nd data in PSAs

406   from the SH (Australia, southern South America (hereafter SSA) and southern Africa

407   (SA)) clearly showed characteristics in these regions and provided insight for tracing

408   dust source–sink paths. For example, $^{87}Sr/^{86}Sr$ ratios in Australian dust samples range

409   from 0.709 to 0.732, and $\varepsilon_{Nd}(0)$ values are between -15 and -3 (Revel-Rolland et al.,

410   2006). Sr-Nd data in Patagonia (39–52°S) of SSA with more radiogenic Nd (-1–1 for

411   $\varepsilon_{Nd}(0)$) (Gaiero, 2007). The aeolian dust from Argentina and Chile is confined to the

412   ranges of 0.7045< $^{87}Sr/^{86}Sr$ <0.7130 and -5 <$\varepsilon_{Nd}(0)$ <3 (Delmonte et al., 2003). The

413   $^{87}Sr/^{86}Sr$ ratios in the sand samples from SA varied between 0.712348 and 0.74716,

414   and the $\varepsilon_{Nd}(0)$ ratios varied between -24.5 and -8.4 (Delmonte et al., 2003; Gili et al.,

415   2021). These Sr-Nd data can very clearly distinguish geographic subgroups for PSAs

416   in SH.

417
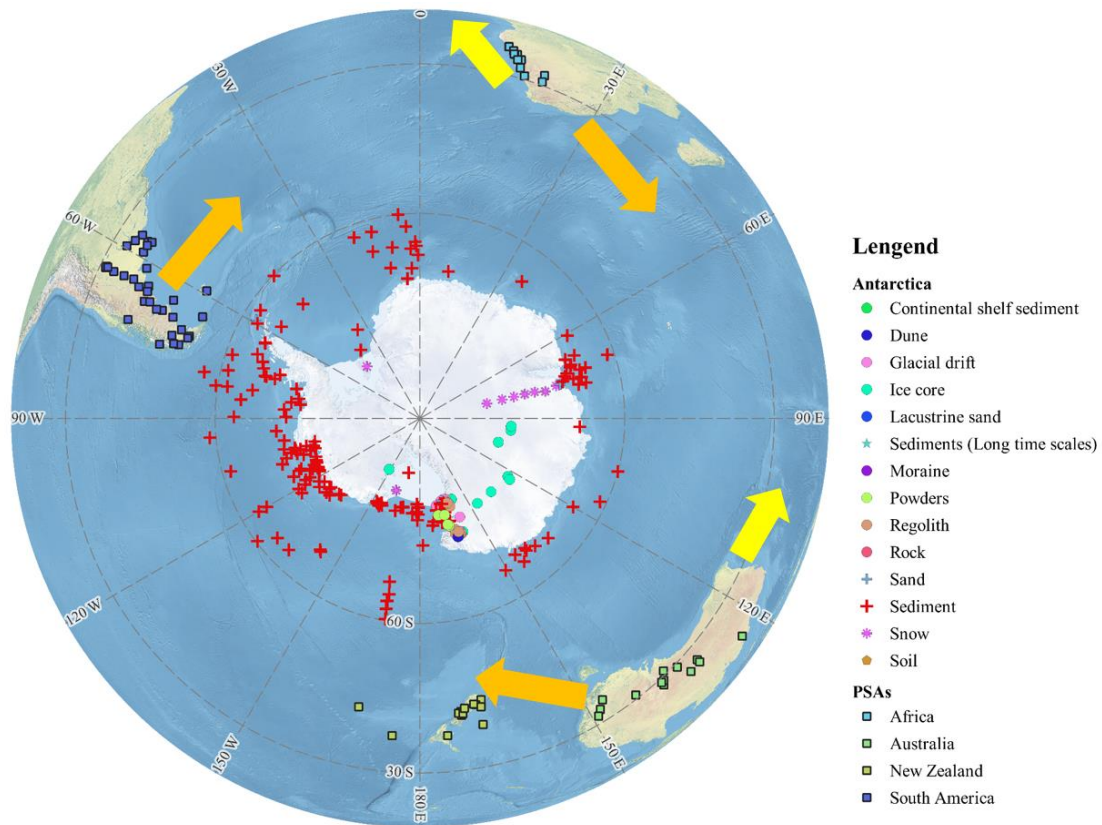
Fig. 7. The locations of the samples were marked in this database for Sr-Nd isotope ratios from Antarctica and PSAs. The dust transport paths are marked with yellow arrows based on previous studies (Gaiero, 2007; Shao et al., 2010; Gili et al., 2021) (this figure was created with ArcGIS).

3.3.1 Sr-Nd data of sediment in Antarctica

Sr-Nd data for the marine sediment (near-core-top samples) from the Circum-Antarctica, terrigenous materials (aeolian dust, glacial drift and dust in ice core) from the AIS are presented in Fig. 8. The ages of these samples were limited to the Holocene. We compared these data with PSA samples from SH. At some sites, if the sample number is >2, we obtained the average Sr-Nd values in this map. For example, for the Pacific sector (146.78°E-67.27°W), $^{87}Sr/^{86}Sr$ values ranged from 0.705281 to 0.725643; $^{87}Sr/^{86}Sr$ values ranged from 0.710616 to 0.738862 for the Indian Ocean sector (20.00°E-146.78°E); $^{87}Sr/^{86}Sr$ values ranged from 0.715989 to 0.741609 for the Atlantic sector (67.27°W-20.00°E) (Hemming et al., 2007). Viewed

432 from Fig. 8, Sr and Nd isotopic contours were determined by inverse distance

433 weighted interpolation, and the numbers of data were >2 in some sites, the averages

434 of surface samples were obtained, the patterns of the two isotopic compositions are

435 consistent in all AIS. Although $^{87}Sr/^{86}Sr$ values differ between sediments from the

436 Circum-Antarctica and sand of PSAs (Australia, SSA and SA), the $^{87}Sr/^{86}Sr$ and $\varepsilon_{Nd}(0)$

437 patterns from the Pacific sector and Indian Ocean sector are relatively consistent with

438 SSA and SA, which can partly explain the aeolian dust contributing to the entire SO.

439 It seems to be abnormal Sr-Nd values that were found in the Ross Sea and Amundsen

440 Sea, which may be attributed to much more samples collecting in the two regions.
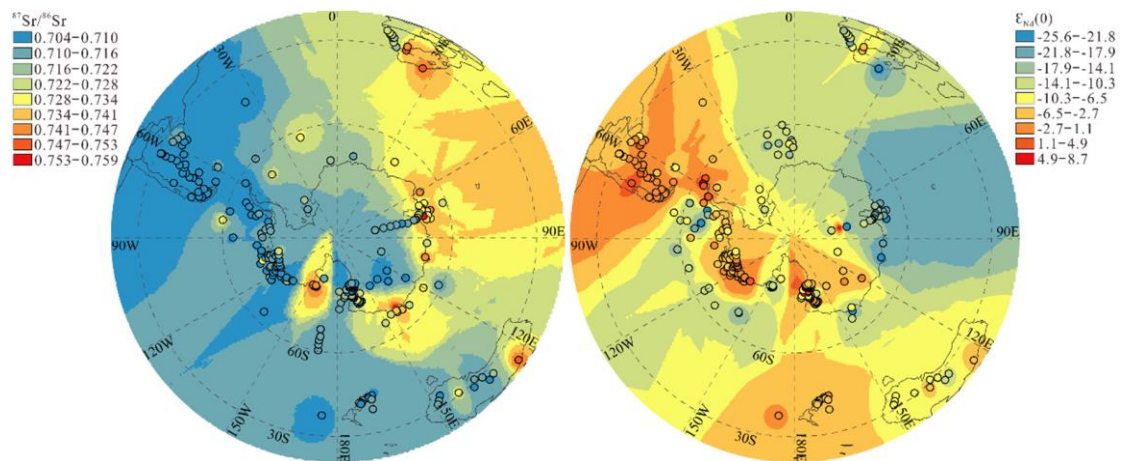
441

442 Fig. 8. Sr versus Nd isotopic compositions for Holocene samples (black circles) at the

443 AIS and its periphery in ice-free areas, and aeolian dust samples (surface samples

444 with no accurate ages) from PSAs in Australia, southern Africa and South America

445 defined by colours, which were determined by inverse distance weighted interpolation

446 using ArcGIS.

447 **3.3.2 Sr-Nd data on the periphery and interior of the Antarctic ice sheet**

448   New Sr-Nd data from coastal and low-elevation sites were measured in ice-free

449 areas near the Filchner–Ronne Ice Shelf, Ross Ice Shelf and Amery Ice Shelf (Fig. 7).

450 Sr-Nd isotope compositions of four sand samples from southern King George Island

451 (South Shetland Islands) in West Antarctica, with less radiogenic $^{87}Sr/^{86}Sr$ values

452 ranging from ~0.703907 to ~0.704157 and relatively higher $\varepsilon_{Nd}(0)$ values ranging

453 from 4.6 to 6.4. The $^{87}Sr/^{86}Sr$ ratios ranged from 0.71135 to 0.72377, and the $\varepsilon_{Nd}(0)$

454 composition ranged from -13.3 to -9.6 from ice-free areas of Inexpressible Island in

455 the Ross Sea, West Antarctica. Based on the Sr-Nd data on our own and the literature

456 (Table 3), we can observe the highest $\varepsilon_{Nd}(0)$ value of >-5.0 in McMurdo and King

457 George Island. The large variations in $^{87}Sr/^{86}Sr$ values and moderate $\varepsilon_{Nd}(0)$ values for

458 Victoria Land and Ross Sea (including Inexpressible Island). The high $^{87}Sr/^{86}Sr$ ratios

459 and low $\varepsilon_{Nd}(0)$ values for the Amery Ice Shelf have the lowest $\varepsilon_{Nd}(0)$ values of <-15.

460 These sub-regions are very close to $\varepsilon_{Nd}(0)$ data from the different sectors of

461 circumpolar sediments (Roy et al., 2007). Therefore, the dataset will be useful for

462 tracing the dust sources or sinks in SO or AIS.

463 However, among these regions, Sr-Nd data have significant differences in some

464 of the endmembers, which are similar, and care must be taken when directly

465 comparing these data to precisely explain the observed isotopic compositions in ice

466 core records. For example, there is overlap of the Sr and Nd isotopic compositions of

467 King George Island, SSA (Patagonia) and McMurdo dry valleys. Sr-Nd data from

468 Inexpressible Island also overlap with the other endmembers (SA, New South Wale

469 and Prydz Bay). Therefore, dust from low-latitude regions (New South Wale and SA)

470 cannot be excluded from East Antarctica (Du et al., 2018; Gili et al., 2021). Another

471 example is the characteristics of snow layers at the Berkner Island ice sheet in western

472 Antarctica. These data can be partly explained by the surface sediment samples from

473 the Weddell Sea sector, with $\varepsilon_{Nd}(0)$ values ranging from -10 to -8 (Hemming et al.,

474 2007). Therefore, the dataset from the SH and AIS demonstrates that multiple mixed

475 sources can be inferred for Antarctic surface snow samples. However, among the data

476 from the entire AIS, Sr-Nd isotopic components were measured in only 29 snow

samples, and there is an urgent need to collect more data in the future.

Information on Sr-Nd data in Antarctic ice cores during the Holocene and glacial-interglacial times is presented by integrating the literature (Du et al., 2022). To obtain enough dust particles, the different age interval samples were merged. For example, each sample represents approximately 40-160 years for the Vostok ice core, which is a few thousand years to obtain a single large-volume sample (Delmonte et al., 2008). Alternatively, several ice core sections from different depths were integrated to obtain a few large samples for the Sr and Nd isotope analyses of the Talos Dome ice core (Delmonte et al., 2010b). A relatively high resolution (spanning between ~ 3 and ~ 30 yrs.) was used in the Taylor Dome ice core (Aarons et al., 2016). Sr-Nd data in the Antarctica deep ice core mainly focus on the coastal and inland areas of the EAIS. As previously mentioned, the dust source is similar to that of the modern samples in the Dome C and Vostok ice cores during the Holocene and interglacial periods, which can be explained by an SSA provenance; an additional hypothesis explains the isotopic signature of Holocene dust in central East Antarctica (Delmonte et al., 2008, Delmonte et al., 2019). Sr-Nd data in the Talos Dome, Taylor Dome and Taylor Glacier ice cores during the Holocene point towards a local dust provenance (Delmonte et al., 2019; Aarons et al., 2016, 2017). Therefore, the Sr and Nd data from East Antarctica ice cores during the Holocene and interglacial periods indicate a well-mixed atmospheric background involving a mixture of two or more sources in the SH (Fig. 8). The study demonstrated that SA emerges as the second most important dust source to East Antarctica during interglacial periods (Gili et al., 2021).

However, the glacial stage (stage 4: ~ 60 ka and stage 6: ~ 160 ka) samples in the Vostok ice core span a very narrow range of Sr compositions ($0.708219 < {}^{87}Sr/{}^{86}Sr < 0.708452$) and Nd compositions ($1.1 < \varepsilon_{Nd}(0) < 5.0$), which can also be explained by

502 the Sr-Nd data in sand samples from southern King George Island ($^{87}Sr/^{86}Sr$ values

503 ranging from ~0.703907 to ~0.704157 and $\varepsilon_{Nd}(0)$ values ranging from 4.6 to 6.4).

504 The $^{87}Sr/^{86}Sr$ and $\varepsilon_{Nd}(0)$ isotopic compositions of dust in the Taylor Glacier ice core

505 samples during the last glacial period indicated that dust may originate from SSA and

506 from potential local source areas in the Ross Sea Sector (Delmonte et al., 2010b;

507 Aarons et al., 2016; Aarons et al., 2017). Therefore, these data suggest that the

508 glacial-period dust in East Antarctic ice cores also contributes from local

509 contributions. However, almost no Sr-Nd data were obtained from West Antarctic

510 deep ice cores, which limits our understanding of the dust transport in the spatial and

511 temporal distribution of the entire AIS. More importantly, the ages of Sr-Nd data in

512 surface aeolian dust from the AIS and PSAs from SH are unknown, which is limited

513 to accurate dust source or sink tracing.

514 **4.Data availability**

515 All datasets and the associated metadata table presented in this study are

516 available through a Big Earth Data Platform for Three Poles. The dataset can be

517 downloaded from https://doi.org/10.11888/Cryos.tpdc.272100) (Du et al., 2022). In

518 this repository, all datasets are provided in Excel spreadsheet format together with

519 metadata files.

520 **5. Conclusions**

521 The maintenance integrated Sr-Nd dataset was presented from the remote three

522 poles, and these data are not easily collected because of the extremely cold and high

523 altitude environment. The dataset is complicated and includes snow, sand, soil, loess,

524 deposits, sediment and other types. We presented case studies of snow, ice core and

525 sediment to demonstrate the Sr-Nd characteristics in the Third Pole glaciers or Arctic

526 and Antarctica ice sheets. These integrated data can provide a new perspective into

present and paleodust sources or sinks from the three poles, more importantly, which clearly emphasizes the following points for potential users of the datasets provided with this paper:

1. This Sr-Nd dataset enables us to map the standardized locations in the remote three poles, while the use of sorting criteria related to the sample location, type or resolution permits us to trace the dust sources or sinks based on their isotopic signatures.

2. For the third pole, each sub-region of Sr-Nd isotopic data was provided, the integration of these data between sand (soil) and snow samples for six sub-regions allowed us to clearly understand the Sr-Nd data characteristics in the Third Pole. The data will be useful for tracing the local or long-distance transported dust of the source and sink for user.

3. The Sr-Nd characteristics in snow (ice) and sediment samples showed that there are significant differences in different sub-regions for the entire Arctic, which would be useful for tracing dust sources or sinks

4. The new data from Arctic and Antarctic samples emphasized the ice-free regions on the periphery of the ice sheets, which may be important local dust sources. However, in particular, Sr-Nd data overlap with the low-latitude regions in Antarctica, the paucity of data in Antarctica is serious and future studies should concentrate on this aspect.

Author contributions. CX, ZD, and SA designed the study, ZD, JY, CX and SA wrote the manuscript. ZD, LW, NW, SW, YL collected the samples in the field and produced the data. ZD, NW, LW, SW, YL, ZW, and XM performed the analysis. All authors contributed to the final form of the manuscript.

Competing interests. The authors declare that they have no conflicts of interest.

552   This work was supported by the Strategic Priority Research Program of the Chinese

553   Academy of Sciences (XAD19070103), the National Natural Science Foundation of

554   China (Grant Nos. 42071086 and 41971088), the National Key Research and

555   Development Program of China (2020YFA0608501), the State Key Laboratory of

556   Cryospheric Science (SKLCS-ZZ-2022) and the Youth Innovation Promotion

557   Association, CAS (2020419). EGRIP is organized by the Center of Ice and Climate at

558   the Niels Bohr Institute and US NSF, Office of Polar Programs. It is supported by

559   funding agencies and institutions in Denmark (A. P. Møller Foundation, UCPH), US

560   (US NSF, Office of Polar Programs), Germany (AWI), Japan (NIPR and ArCS),

561   Norway (BFS), Switzerland (SNF), France (IPEV, IGE), and China (CAS). We thank

562   all people involved in snow samples collecting from central Arctic Ocean by the

563   expedition of the Research Vessel Polarstern for their great logistical supports during

564   MOSAiC in 2019–2020. We also thank the Chinese Arctic and Antarctic

565   Administration contributing to the part of MOSAiC.

566

567

568 **References:**

569 Aarons, S., Aciego, S., Gabrielli, P., Delmonte, B., Koornneef, J., Wegner, A., and Blakowski, M.: The

570 impact of glacier retreat from the Ross Sea on local climate: Characterization of mineral dust in the

571 Taylor Dome ice core, East Antarctica, Earth Planet. Sc. Lett, 444, 34–44,

572 https://doi.org/10.1016/j.epsl.2016.03.035, 2016.

573 Aarons, S. M., Aciego, S. M., Arendt, C. A., Blakowski, M. A., Steigmeyer, A., Gabrielli, P.,

574 SierraHernández, M. R., Beaudon, E., Delmonte, B., Baccolo, G., May, N. W., and Pratt, K. A.: Dust

575 composition changes from Taylor Glacier (East Antarctica) during the last glacial-interglacial transition:

576 A multi-proxy approach, Quat. Sci. Rev, 162, 60-71, https://doi.org/10.1016/j.quascirev.2017.03.011,

577 2017.

578 Abbott, A. N., Löhr, S. C., Payne, A., Kumar, H., and Du, J.: Widespread lithogenic control of marine

579 authigenic neodymium isotope records? Implications for paleoceanographic reconstructions.

580 Geochimica et Cosmochimica Acta, 319, 318-336. https://doi.org/10.1016/j.gca.2021.11.021.

581 Asahara, Y., Takeuchi, F., Nagashima, K., Harada, N., Yamamoto, K., Oguri, K., Tadai, O.: Provenance

582 of terrigenous detritus of the surface sediments in the Bering and Chukchi Seas as derived from Sr and

583 Nd isotopes: implications for recent climate change in the Arctic regions. Deep Sea Res. Part II 61–64,

584 155–171. https://doi.org/10.1016/j.dsr2.2011.12.004, 2012.

585 Bayon, G., Freslon, N., Germain, Y., Bindeman, I.N., Trinquier, A., Barrat, J.A.: A global survey of

586 radiogenic strontium isotopes in river sediments. Chem. Geol. 559, 119958.
587 https://doi.org/10.1016/j.epsl.2022.117490, 2021.

588 Biscaye, P.E., Grousset, F.E., Revel, M., Van der Gaast, S., Zielinski, G.A., Vaars, A., and Kukla, G.:
589 Asian provenance of glacial dust (stage 2) in the Greenland Ice Sheet Project 2 ice core, Summit,
590 Greenland. J. Geophys. Res.-Oceans, 102, 26765-26781. https://doi.org/10.1029/97JC01249, 1997.

591 Blakowski, M.A., Aciego, S.M., Delmonte, B., Baroni, C., Salvatore, M.C., Sims, K.W.W.: A
592 Sr–Nd–Hf isotope characterization of dust source areas in Victoria Land and the McMurdo Sound
593 sector of Antarctica. Quat. Sci. Rev. 141, 26–37. https://doi.org/10.1016/j.quascirev.2016.03.023.

594 Blanchet C L.: A database of marine and terrestrial radiogenic Nd and Sr isotopes for tracing
595 earth-surface processes. Earth Syst. Sci. Data, 11(2):741-759. https://doi.org/10.5194/essd-11-741-2019,
596 2019.

597 Bory, J. M., Biscaye, P. E., Svensson, A., and Grousset, F. E.: Seasonal variability in the origin of
598 recent atmospheric mineral dust at NorthGRIP, Greenland. Earth Planet. Sc. Lett, 196(3-4):123-134.
599 https://doi.org/10.1016/S0012-821X(01)00609-4, 2002.

600 Bory, A.M., Biscaye, P.E., Piotrowski, A.M., Steffensen, J.P.: Regional variability of ice core dust
601 composition and provenance in Greenland. Geochem. Geophy. Geosy, 4.
602 https://doi.org/10.1029/2003GC000627, 2003a.

603 Bory, A.J.M., Biscaye, P.E., Grousset, F.E.: Two distinct seasonal Asian source regions for mineral dust
604 deposited in Greenland (NorthGRIP). Earth Sci. Rev, 30. https://doi.org/10.1029/2002GL016446,
605 2003b.

606 Bory, A., Wolff, E., Mulvaney, R., Jagoutz, E., Wegner, A., Ruth, U., and Elderfield, H.: Multiple
607 sources supply eolian mineral dust to the atlantic sector of coastal antarctica: evidence from recent
608 snow layers at the top of Berkner island ice sheet, Earth Planet. Sci. Lett, 291(1-4), 138-148,
609 https://doi:10.1016/j.epsl.2010.01.006, 2010.

610 Chen, J., Li, G., Yang, J., Rao, W., Lu, H., Balsam, W., Sun, Y., and Ji, J.: Nd and Sr isotopic
611 characteristics of Chinese deserts: implications for the provenances of Asian dust. Geochimica Et
612 Cosmochimica Acta, 71, 3904-3914, https://doi.org/10.1016/j.gca.2007.04.033, 2007.

613 Delmonte, B., Quaternary variations and origin of continental dust in East Antarctica, PhD Thesis,
614 Università degli Studi di Siena / Université Joseph Fourier - Grenoble 1, 2003.

615 Delmonte, B., Andersson, P.S., Hansson, M., Schoberg, H., Petit, J.R., Basile-Doelsch, I., and Maggi,
616 V.: Aeolian dust in East Antarctica (EPICA-Dome C and Vostok): provenance during glacial ages over
617 the last 800 kyr. Geophys. Res. Lett, 35 (7), L07703, https://doi:10.1029/02008GL033382, 2008.

618 Delmonte, B., Andersson, P.S., Schoberg, H., Hansson, M., Petit, J.R., Delmas, R., Gaiero, D.M.,
619 Maggi, V., and Frezzotti, M.: Geographic provenance of Aeolian dust in East Antarctica during
620 Pleistocene glaciations: preliminary results from Talos Dome and comparison with East Antarctic and
621 new Andean ice core data. Quat. Sci. Rev, 29, 256–264, https://doi.org/10.1016/j.quascirev.2009.05.010,
622 2010a.

623 Delmonte, B., Baroni, C., Andersson, P.S., Schöberg, H., Hansson, M., Aciego, S., Petit, J.-R., Albani,
624 S., Mazzola, C., Maggi, V., and Frezzotti, M.: Aeolian dust in the Talos Dome ice core (East Antarctica,
625 Pacific/Ross Sea sector): Victoria Land versus remote sources over the last two climate cycles. J. Quat.
626 Sci, 25 (8), 1327–1337, https://doi.org/10.1002/jqs.1418, 2010b.

627 Delmonte, B., Baroni, C., Andersson, P. S., Narcisi, B., Salvatore, M. C., Petit, J. R., Scarchilli, C.,
628 Frezzotti, M., Albani, S., and Maggi, V.: Modern and Holocene aeolian dust variability from Talos
629 Dome (Northern Victoria Land) to the interior of the Antarctic ice sheet, Quaternary Sci. Rev, 64,

630   76–89, doi:10.1016/j.quascirev.2012.11.033, 2013.

631   Delmonte, B., Paleari, C. I., Andò, S., Garzanti, E., Andersson, P. S., Petit, J. R., Crosta, X., Narcisi, B.,

632   Baroni, C., Salvatore, M., Baccolo, G., and Maggi.: Causes of dust size variability in central East

633   Antarctica (Dome B): Atmospheric transport from expanded South American sources during Marine

634   Isotope Stage 2. Quaternary Sci. Rev, 168, 55–68, https://doi.org/10.1016/j.quascirev.2017.05.009,

635   2017.

654   Delmonte, B., Winton, H., Baroni, M., Baccolo, G., Hansson, M., Andersson, P., Baroni, C., Salvatore,

655   M., Lanci, L., and Maggi, V.: Holocene dust in East Antarctica: provenance and variability in time and

656   space. Holocene, 30 (4), 546-558, https://doi.org/10.1177/0959683619875188, 2019.

657   Dong, Z., Shao, Y., Qin, D., Kang, S., Wei, W., Wang, X., and Wang, S.: Hf-Nd-Sr isotopic composition

658   as fingerprint for long-range transported eolian dust deposition in glacier snowpack of eastern Tibetan

659   Plateau. J. Geophys. Res, 123, 7013–7023, https://doi.org/10.1029/2018JD028581, 2018.

660   Du, Z., Xiao, C., Liu, Y., Wu, G.: Geochemical characteristics of insoluble dust as a tracer in an ice

661   core   from   Miaoergou   Glacier,   east   Tien   Shan.   Glob.   Planet.   Chang,   127,   12-21.

662   http://doi.org/10.1016/j.gloplacha.2015.01.011, 2015.

663   Du, Z., Xiao, C., Ding, M., and Li, C.: Identification of multiple natural and anthropogenic sources of

664   dust in snow from Zhongshan Station to Dome A, East Antarctica. J. Glaciol, 64: 855–865,

665   https://doi.org/10.1017/jog.2018.72, 2018.

666   Du, Z., Xiao, C., Wang, Y., Liu, S., and Li, S.: Dust provenance in Pan-third pole modern glacierized

667   regions: What   is   the   regional   source?.   Environmental   Pollution,   250(JUL.):   762-772,

668   https://doi.org/10.1016/j.envpol.2019.04.068, 2019a.

669   Du, Z., Xiao, C., Dou, T., Li, S., An, H., Liu, S., and Liu K.: Comparison of Sr–Nd–Pb isotopes in

670   insoluble dust between northwestern China and high-latitude regions in the Northern Hemisphere.

671   Atmospheric Environment, 214:116837, https://doi.org/10.1016/j.atmosenv.2019.116837, 2019b.

672   Gaiero, D.M., Brunet, F., Probst, J.L., Depetris, P.J.: A uniform isotopic and chemical signature of dust

673   exported from Patagonia: rock sources and occurrence in southern environments. Chem. Geol. 238 (1),

674   107-120, https://doi.org/10.1016/j.chemgeo.2006.11.003, 2007.

675   Gili, S., Vanderstraeten, A., Chaput, A., King, J., Gaiero, D., Delmonte, B., Vallelonga, P., Formenti, P.,

676   Di Biagio, C., Cazanau, M. and Pangui, E.: Southern Africa: The Missing Piece To The Dust

677   Provenance Puzzle of East Antarctica? Communications Earth & Environment, 2021.

678   Grousset, F. E., Biscaye, P. E., Revel, M.., Petit, J., Pye, K., Joussaume, S., and Jouzel, J.: Antarctic

679   (Dome C) ice-core dust at 18 k.y. B. P.: isotopic constraints on origins, Earth Planet. Sci. Lett, 111,

680   175–182, https://doi.org/10.1016/0012-821X(92)90177-W, 1992.

681   Grousset, F. E., Parra, M., Bory, A., Martinez, P., Bertrand, P., Shimmield, G and Ellam, R. M.: Saharan

682   wind regimes traced by the Sr–Nd isotopic composition of subtropical Atlantic sediments: last glacial

683   maximum vs today, Quaternary Sci. Rev, 17, 395–409, https://doi.org/10.1016/S0277-3791(97)00048-6,

684   1998.

685   Han, C., Hur, S. D., Han, Y., Lee, K., Hong, S., Erhardt, T., Fischer, H., Svensson, A., Steffensen, JP.,

686   and Vallelonga, P.: High-resolution isotopic evidence for a potential Saharan provenance of Greenland

687   glacial dust. Sci Rep, 8, 15582, https://doi.org/10.1038/s41598-018-33859-0, 2018.

688   Hemming, S.R., van de Flierdt, T., Goldstein, S.L., Franzese, A.M., Roy, M., Gastineau, G., Landrot,

689   G.: Strontium isotope tracing of terrigenous sediment dispersal in the Antarctic Circumpolar Current:

690   implications for constraining frontal positions. Geochem. Geophys. Geosyst, 8 (6), Q06N13,

691   https://doi:10.1029/2006GC001441, 2007.

692   Jacobsen, S.B., Wasserburg, G.J. (1980) Sm-Nd evolution of chondrites. Earth Planet. Sci. Lett. 50,
693   139-155.

694   Jonell, T.N., Li, Y., Blusztajn, J., Giosan, L., Clift, P.D.: Signal or noise? Isolating grain size effects on
695   Nd and Sr isotope variability in Indus delta sediment provenance. Chem. Geol. 485, 56e73.
696   https://doi.org/10.1016/j.chemgeo.2018.03.036, 2018.

697   Lambert, F., Kug, J. S., Park, R. J., Mahowald, N., Winckler, G., Abe-Ouchi, A., and Lee, J. H.: The
698   role of mineral-dust aerosols in polar temperature amplification, Nat. Clim. Change, 3, 487– 491,
699   https://doi.org/10.1038/nclimate1785, 2013.

700   Li, X., Che, T., Li, X., Wang, L., Duan, A., Shangguan, D., Pan, X., Fang, M., and Bao, Q.: CASEarth
701   Poles: Big data for the Three Poles, B. Am. Meteorol. Soc., 101, E1475–E1491, 2020

702   Lin, Y. C., Feng, J. L.: Aeolian dust contribution to the formation of alpine soils at Amdo (Northern
703   Tibetan Plateau). Geoderma 259, 104e115. https://doi.org/10.1016/j.geoderma.2015.05.012, 2015.

704   Lupker, M., Aciego, S.M., Bourdon,B., Schwander,J., and Stocker, T.F.: Isotopictracing(Sr, Nd, U and
705   Hf) of continental and marine aerosols in an 18th century section of the Dye-3 ice core (Greenland).
706   Earth Planet. Sci. Lett, 295. http://dx.doi.org/10.1016/j.epsl.2010.04.010, 2010.

707   Maccali, J., Hillaire-Marcel, C., Not, C.: Radiogenic isotope (Nd, Pb, Sr) signatures of surface and sea
708   ice-transported sediments from the Arctic Ocean under the present interglacial conditions. Polar
709   Research, 37(1):1442982, 2018. https://doi.org/10.1080/17518369.2018.1442982.

710   Meinhardt, A.K., Pahnke, K., Böning, P., Schnetger, B., Brumsack, H.J.: Climate change and response
711   in bottom water circulation and sediment provenance in the central Arctic Ocean since the last glacial.
712   Chem. Geol. 427, 98–108. http://dx.doi.org/10.1016/j.chemgeo.2016.02.019, 2016.

713   Nagatsuka, N., Takeuchi, N., Nakano, T., Kokado, E., and Li, Z.: Sr, Nd, and Pb stable isotopes of
714   surface dust on Urumqi glacier No.1 in western China. Ann. Glaciol., 51(56), 95–105.
715   https://doi.org/10.3189/172756411795931895, 2010.

716   Nagatsuka, N., Takeuchi, N., Uetake, J., Shimada, R., Onuma, Y., Tanaka, S., and Nakano, T.:
717   Variations in Sr and Nd isotopic ratios of mineral particles in cryoconite in Western Greenland.
718   Frontiers in Earth Science 4, 93, https://doi.org/10.3389/feart.2016.00093, 2016.

719   Rao, W.B., Yang, J.D., Chen, J., Li, G.L.: Sr–Nd isotope geochemistry of eolian dust of the
720   arid-semiarid areas in China: implications for loess provenance and monsoon evolution. Chin. Sci. Bull.
721   51 (12), 1401–1412, 2006. https://doi.org/10.1007/s11434-006-2008-1.

722   Revel, M., Sinko, J. A., Grousset, F. E., and Biscaye, P. E.: Sr and Nd isotopes as tracers of North
723   Atlantic   lithic   particles: Paleoclimatic   implications,   Paleoceanography,   11,   95–113,
724   https://doi.org/10.1029/95PA03199, 1996.

725   Revel-Rolland M, De Deckker, P., Delmonte, B., Hesse, P.P., Magee, J.W., Basile-Doelsch, Grousset, F.,
726   and Bosch, D.: Eastern Australia: A possible source of dust in East Antarctica interglacial ice. Earth
727   Planet. Sc. Lett, 249(1–2): 1–13, https://doi.org/10.1016/j.epsl.2006.06.028, 2006.

728   Robinson, S., Ivanovic, R., Flierdt, T. Van De, Blanchet, L., Tachikawa, K., Martin, E.E., Falco, C.P.C.,
729   Williams, T., Gregoire, L., Plancherel, Y., Jeandel, C., Arsouze, T.: Global continental and marine
730   detrital εNd: an updated compilation for use in understanding marine Nd cycling. Chem. Geol. 567,
731   120119. https:// doi.org/10.1016/j.chemgeo.2021.120119, 2021.

732   Roy, M., van de Flierdt, T., Hemming, S. R., and Goldstein, S. L.: ^{40}Ar/^{39}Ar ages of hornblende grains
733   and bulk Sm/Nd isotopes of circum-Antarctic glacio-marine sediments: Implications for sediment
734   provenance   in   the   southern   ocean,   Chem.   Geol.,   244,   507–519,
735   https://doi.org/10.1016/j.chemgeo.2007.07.017, 2007.

Shao, Y., Wyrwoll, K.H., Chappell, A., Huang, J., Lin, Z., McTainsh, G.H., Yoon, S.: Dust cycle: an emerging core theme in Earth system science. Aeolian Res. 2 (4), 181–204. https://doi.org/10.1016/j.aeolia.2011.02.001, 2011.

Simonsen, M. F., Baccolo, G., Blunier, T., Borunda, A., Delmonte, B., Frei, R., Goldstein, S., Grinsted, A., Kjær, A.A., Sowers, T., Svensson, A., Vinther, B., Vladimirova, D., Winckler, G., Winstrup, M., and Vallelonga, P.: East Greenland ice core dust record reveals timing of Greenland ice sheet advance and retreat. Nature Communications, 10(1):1-8, https://doi.org/10.1038/s41467-019-12546-2, 2019.

Skiles, S.M., Flanner, M., Cook, J.M. Dumont, M., Painter, T. H.: Radiative forcing by light-absorbing particles in snow. Nature Clim Change 8, 964–971. https://doi.org/10.1038/s41558-018-0296-5, 2018.

Struve, T., Pahnke, K., Lamy, F., Wengler, M., Böning, P., Winckler, G.: A circumpolar dust conveyor in the glacial Southern Ocean. Nature Communications, 11(1), 1–11. https://doi.org/10.1038/s41467-020-18858-y, 2020.

Svensson, A., Biscaye, P.E., Grousset, F.E.: Characterization of late glacial continental dust in the Greenland Ice Core Project ice core. J. Geophys. Res.: Atmosphere, 105, 4637-4656, https://doi.org/10.1029/1999JD901093, 2000.

Tütken, T., Eisenhauer, A., Wiegand, B., Hansen, B.T., 2002. Glacial–interglacial cycles in Sr and Nd isotopic composition of Arctic marine sediments triggered by Svalbard/Barents Sea ice sheet. Marien Geology 182, 351–372. https://doi.org/10.1016/S0025-3227(01)00248-1.

Újvári, G., Stevens, T., Svensson, A., Klötzli, U.S., Manning, C., Németh, T., Kovács, J., Sweeney, M.R., Gocke, M., Wiesenberg, G.L.B., Markovic, S.B., Zech, M.: Two possible source regions for central Greenland last glacial dust. Geophys. Res. Lett. 42, 10,399–310, 408, https://doi.org/10.1002/2015GL066153, 2015.

Walter, H.J., Hegner, E., Diekmann, B., Kuhn, G., van der Loeff, M.M.R.: Provenance and transport of terrigenous sediment in the South Atlantic Ocean and their relations to glacial and interglacial cycles: Nd and Sr isotopic evidence. Geochimica Et Cosmochimica Acta 64 (22), 3813–3827. https://doi.org/10.1016/S0016-7037(00)00476-2, 2000.

Wei, T., Dong, Z., Kang, S., Qin, X., Guo, Z.: Geochemical evidence for sources of surface dust deposited on the Laohugou glacier, Qilian Mountains. Appl. Geochem. 79, 1-8. http://doi.org/10.1016/j.apgeochem.2017.01.024, 2017.

Wei, T., Dong, Z., Kang, S., Rostami, M., Ulbrich, S., and Shao, Y.: Hf-Nd-Sr isotopic fingerprinting for aeolian dust deposited on glaciers in the northeastern Tibetan Plateau region. Glob. Planet. Chang, 177, 69–80, https://doi.org/10.1016/j.gloplacha.2019.03.015, 2019.

Wei, T., Brahney, J., Dong, Z., Kang, S., Zong, C., Guo, J., Yang, Lin., Qin, X.: Hf-Nd-Sr Isotopic Composition of the Tibetan Plateau Dust as a Fingerprint for Regional to Hemispherical Transport. Environmental Science & Technology, 55(14). https://doi.org/10.1021/acs.est.0c04929, 2021.

Wu, G., Zhang, C., Zhang, X., Tian, L., Yao, T.: Sr and Nd isotopic composition of dust in Dunde ice core, Northern China: implications for source tracing and use as an analogue of long-range transported Asian dust. Earth Planet. Sci. Lett, 299 (3), 409-416. http://doi.org/10.1016/j.epsl.2010.09.021, 2010.

Xie, Y., Liu, L., Kang, C., Chi, Y.: Sr-Nd isotopic characteristics of the Northeast Sandy Land, China and their implications for tracing sources of regional dust. Catena 184, 104303. https://doi.org/10.1016/j.catena.2019.104303, 2020.

Xu, J., Yu, G., Kang, S., Hou, S., Zhang, Q., Ren, J., Qin, D.: Sr-Nd isotope evidence for modern aeolian dust sources in mountain glaciers of western China. J. Glaciol, 58 (211), 859-865. http://doi.org/10.3189/2012JoG12J006, 2012.

Winton, V. H. L., Edwards, R., Delmonte, B., Ellis, A., Andersson, P. S., Bowie, A., Bertler, N. A. N., Neff, P., and Tuohy, A.: Multiple sources of soluble atmospheric iron to Antarctic waters, Global Biogeochem. Cy., 30, 421–437, https://doi.org/10.1002/2015GB005265, 2016.

Table 1. Data distribution locations and sample types for $^{87}Sr/^{86}Sr$ and $\varepsilon_{Nd}(0)$ from 90 references.

Region	Characteristics	Data characteristics	Attribution/ harmonization of coordinates	Attribution sorting of criteria	Number of data points
Third Pole					**485**
Kunnun Mountain (Pamirs)	Peer-reviewed publications	Snow, River Sediment, Moraine	Yes	Yes	39
Tibetan Plateau	Peer-reviewed publications and own research articles	Snow, Soil, Sand, River Sediment	Yes	Yes	102
Himalaya Mountain	Peer-reviewed publications	Snow, River Sediment	Yes	Yes	14
Qilian Mountain	Peer-reviewed publications and own research articles	Snow, Ice, River Sediment, Soil, Moraine	Yes	Yes	66
Hengduan Mountain	Peer-reviewed publications	Snow, Soil	Yes	Yes	17
Western Chinese Deserts	Peer-reviewed publications and own research articles	Sand, Dune, Fluvial, Lacustrine, Proluvial	Yes	Yes	219
Chinese Loess Plateau	Peer-reviewed publications and own research articles	Loess	Yes	Yes	21
Others (Qinling and Linxia Basin)	Peer-reviewed publications	River sediment	Yes	Yes	7
Pan-third Pole	Peer-reviewed publications and own research articles	Snow, Ice, Sand, Soil, Loess, Moraine, Lacustrine, Dune	Yes	Yes	**259**
Arctic					**727**
Greenland ic sheet	Peer-reviewed publications, own research articles and own measurements	Snow, Ice, Cryoconite, Sand, Sediment, Rock	Yes	Yes	186
Svalbard (Atlantic Ocean)	Peer-reviewed publications and own research articles	Snow, Sand, Sediment	Yes	Yes	32
Arctic Ocean	Peer-reviewed publications, own research articles and own measurements	Snow, Sediment, Waters	Yes	Yes	496
Others (Rivers and Alaska)	Peer-reviewed publications and own research articles	Snow, Soil (Sand), River Sediment	Yes	Yes	13
Antarctica					**777**
East Antarctica	Peer-reviewed publications and own research articles	Snow, Ice, Sand, Regolith, Glacial drift, Dune, Moraine, Aeolian deposit, Rock, Sediment	Yes	Yes	298
West Antarctica	Peer-reviewed publications and own measurements	Snow, Ice, Sand, Rock, Sediment	Yes	Yes	44
Southern Ocean	Peer-reviewed publications	Sediment	Yes	Yes	435

PSA in Southern Hemisphere					**181**
South America	Peer-reviewed publications	Loess, Soil, Sediment, Aeolian dust	Yes	Yes	57
Southern Africa	Peer-reviewed publications	Aeolian dust, Loess, Sediment deposit, Aerosol	Yes	Yes	53
Australia	Peer-reviewed publications	Sand, Loess, Dune, Lacustrine, Sediment	Yes	Yes	24
New Zealand	Peer-reviewed publications	Loess, Aeolian deposits	Yes	Yes	16
Others	Peer-reviewed publications	Sediment	Yes	Yes	31
Grain sizes	Peer-reviewed publications	Sand, Loess, Sediment, Rock	Yes	Yes	**206**
Methods	Peer-reviewed publications	Loess, Sand, Cryoconite, Rock, Moraine, Dust, Aerosol, River sediment	Yes	Yes	**212**
Grand total					**2847**

785

786 Table 2. Snow, sand and soil samples were located in the third pole glaciers and PSAs of dust
787 generation. Headers from left to right: Label: the number of glaciers; Sub-regions; Glacier name; Site
788 name: name of the sampling site where the samples were taken; Longitude and Latitude; sampling
789 location; Sample type: Snow, sand or soil; Elevation: m a.s.l; Isotopic ratios of Sr and $\varepsilon_{Nd}(0)$; Ref.:
790 reference publications. The different colours represent different sub-regions.

Label	Glacier name	Sub-regions	Latitude (° N)	Longitude (° E)	Mountains	Sample type	Elevation (m a.s.l)	$^{86}Sr/^{87}Sr$	$\varepsilon_{Nd}(0)$	Ref
1	Musidao	Region I	47.10	85.55	Altai	Snow	3605	0.713185–0.713571	-6.55—-4.80	Xu et al., 2012
2	Muztagata		38.28	75.10	East Pamirs	Snow	6365	0.717187–0.717415	-10.3—-8.4	Xu et al., 2012
3	Tienshan No. 1	Region II	43.12	86.82	Tien Shan	Snow, dust	4063	0.719404–0.721728	-10.9—-6.9	Nagatsuka et al., 2010; Xu et al., 2012
4	Miaoergou		43.06	94.32	Tien Shan	Snow, Ice, Cryoconite	3100–4512	0.710284–0.720825	-11.6—-7.3	Du et al., 2015; Wei et al., 2019
5	Yuzhufeng Glacier		35.66	94.24	Kunlun	Snow	4300–4720	0.714821–0.716757	-16.6—-11.8	Wei et al., 2019
6	Zangsegangri		34.27	85.85	Qiangtang	Snow	6226	0.717352–0.718328	-12.9—-9.2	Xu et al., 2012
7	Guoqu	Region III	33.58	91.20	Tanggula	Snow	5765	0.717546–0.721786	-10.2—-9.5	Xu et al., 2012
8	Dongkemadi		33.10	92.10	Tanggula	Snow	5700	0.713192	-10.5	Xu et al., 2012
9	Zadang		30.47	90.65	Nyainqentanglha	Snow	5758	0.718285–0.721305	-12.9—-11.1	Xu et al., 2012
10	Jiemayangzong		30.22	82.17	Himalaya	Snow	5558	0.72671–0.740694	-14.3—-10.5	Xu et al., 2012
11	Yala	Region IV	28.23	85.62	Himalaya	Snow	5190	0.740112	-15.68	Xu et al., 2012
12	East Rongbuk		28.10	86.97	Himalaya	Snow	6525	0.728057–0.757407	-28.1—-14.7	Xu et al., 2012
13	Laohugou Glacier No.12		39.43	96.53	Qilian	Snow	4288–5026	0.720448–0.723303	-15.7—-9.5	Xu et al., 2012; Wei et al., 2019
14	Dunde ice cap		38.10	96.40	Qilian	Ice	5325	0.715220–0.721874	-11.1—-9.9	Wu et al., 2010
15	Qiyi Glacier 1	Region V	39.24	97.76	Qilian	Snow	4500–4750	0.712349–0.722751	-13.7—-8.6	Dong et al., 2018
16	Shiyi Glacier		38.21	99.88	Qilian	Snow	3928–4152	0.721032–0.721711	-14.0—-13.8	Wei et al., 2019
17	Dabanshan		37.36	101.40	Qilian	Snow	3593–3625	0.723105–0.725015	-12.1—-12.0	Wei et al., 2019
18	Lenglongling Glacier		37.52	101.90	Qilian	Snow	3558–3992	0.719084–0.728414	-10.9—-7.0	Dong et al., 2018
19	Dagu Glacier		32.12	102.43	Hengduan	snow	3520–3701	0.719216–0.721102	-16.9—-12.3	Dong et al., 2018
20	Hailuogou Glacier	Region VI	29.33	101.57	Hengduan	snow	3010–3850	0.722805–0.728326	-17.1—-12.0	Dong et al., 2018
21	Demula Glacier		29.37	97.00	Hengduan	Snow	5404	0.729095–0.735863	-17.1—-14.2	Xu et al., 2012
22	Baishui Glacier No.1		27.10	100.20	Hengduan	Snow	4338–4747	0.717145–0.719881	-13.8—-11.4	Xu et al., 2012; Dong et al., 2018

791
792
793
794
795
796

Table 3. Snow, cryoconite, sand, soil and sediment samples located in the Arctic. Headers from left to right: Label; Subregions; name of the sampling site where the samples were taken; Sample type: Snow, Cryoconite, sand and soil; Ref.: reference publications.

Label	Subregion	Location	Sample type	Time interval	Size fraction	Ref
1	GrISS	East GrIS; North GrIS	snowpit	2017/2018; early-1995	>0.2 μm; <45 or 38 μm	This study; Bory et al., 2002
2	GrIS-S	East GrIS; West GrIS	Cryoconite, Moraine, Englacial dust, Sand, Rock, Sediment	NO	Bulk	This study; Nagatsuka et al., 2016; Simonsen et al., 2019
3	SV	Ny-Ålesund	Snow, Sand, Soil; Sediment	NO	Bulk; <100 μm	Tütken et al., 2002; Maccali et al., 2018; Du et al., 2019b
4	AO	Arctic Ocean	Snow	2016	Bulk	This study; Du et al., 2019b
5	AOSI	Arctic Ocean	Sea ice sediment	NO	<100 μm	Eisenhauer et al., 1999; Tütken et al., 2002
6	AOSed	Arctic Ocean	Sediment	NO	Bulk; <100 μm	Eisenhauer et al., 1999; Tütken et al., 2002; Maccali et al., 2018
7	BS	Arctic Ocean	Sediment	NO	<100 μm	Tütken et al., 2002; Maccali et al., 2018
8	KS	Arctic Ocean	Sediment	NO	<100 μm	Tütken et al., 2002; Maccali et al., 2018
9	LS	Arctic Ocean	Sediment	NO	<100 μm; Bulk	Eisenhauer et al., 1999; Maccali et al., 2018
10	ESS	Arctic Ocean	Sediment	NO	<100 μm	Bazhenova et al., 2017; Maccali et al., 2018
11	BCS	Arctic Ocean	Sediment	NO	<100 μm; Detrital	Asahara et al., 2012; Bazhenova et al., 2017; Maccali et al., 2018; Du et al., 2019b
12	CAA	Arctic Ocean	Sediment	NO	<100 μm	Asahara et al., 2012; Bazhenova et al., 2017; Maccali et al., 2018